Review

Recent Progress in On-Chip Erbium-Based Light Sources

Bo Wang [1], Peiqi Zhou [2] and Xingjun Wang [1,3,4,5,*]

1   State Key Laboratory of Advanced Optical Communication Systems and Networks, School of Electronics, Peking University, Beijing 100871, China
2   National Information Optoelectronics Innovation Center, Wuhan 430074, China
3   Frontier Science Center for Nano-Optoelectronics, Peking University, Beijing 100871, China
4   Peking University Yangtze Delta Institute of Optoelectronics, Nantong 226010, China
5   Peng Cheng Laboratory, Shenzhen 518055, China
*   Correspondence: xjwang@pku.edu.cn

Featured Application: Silicon photonics.

Abstract: In recent years, silicon photonics has achieved great success in optical communication area. More and more on-chip optoelectronic devices have been realized and commercialized on silicon photonics platform, such as silicon-based modulators, filters and detectors. However, on-chip light sources are still not achieved because that silicon is an indirect bandgap material. To solve this problem, the rare earth element erbium (Er) is considered, which emits light covering 1.5 μm to 1.6 μm and has been widely used in fiber amplifiers. Compared to Er-doped fiber amplifiers (EDFA), the Er ion concentration needs to be more than two orders higher for on-chip Er-based light sources due to the compact size integration requirements. Therefore, the choice of the host material is crucially important. In this paper, we review the recent progress in on-chip Er-based light sources and the advantages and disadvantages of different host materials are compared and analyzed. Finally, the existing challenges and development directions of the on-chip Er-based light sources are discussed.

Keywords: Er-based light source; on-chip waveguide amplifier; on-chip waveguide laser

1. Introduction

With the rapid development of the silicon-based microelectronics technology in accordance with the Moore's Law, the feature size of the devices is reduced to less than ten nanometers [1]. Nevertheless, the power consumption and the heat dissipation of the devices have become a non-negligible problem, which restricts the development of microelectronics technology. In addition, it is hard to further reduce the size of the microelectronic devices, increase the integration of the chips, and improve the performance of the devices [2]. Therefore, the microelectronics technology is currently difficult to meet the increasingly high requirements of the information society.

In recent years, silicon photonics has attracted great attention and research effort due to its potential for low-cost integration of complementary metal–oxide–semiconductor (CMOS) technology and the small size of silicon-based photonic devices. It combines photonics technology and microelectronics technology to achieve larger transmission bandwidth and higher communication speed, which has been widely used in on-chip optical communication. In recent years, the possible experimental implementation and on photonic bandgap have provided a reliable way to transmit entanglement over long distance and high-performance computing, which indicates silicon photonic technologies also have potential application in frontier domains, such as quantum technology and neural networks [3–8]. Some key devices in silicon photonics, such as modulators, detectors, wavelength division multiplexers, filters and other functional devices have been realized

and gradually industrialized [9–13]. However, the only thing that has not been completely solved at present is the silicon-based light sources because of the indirect band properties of silicon [14]. To solve this problem, there are mainly three methods: epitaxial III-V light sources, heterogeneous III-V light sources and Er-based light sources.

1.1. Epitaxial III-V Light Sources

III-V compound semiconductor lasers have developed rapidly in recent decades and are gradually commercialized. Silicon-based epitaxial growth of III-V compound semiconductor light sources have been pursued for many decades for the potential to integrate with other silicon-based optoelectronic devices. However, compared with Si, III-V compound materials have large lattice mismatches and thermal expansion coefficient mismatches, which results in a threading or misfit dislocation density of 10^8–10^{10} cm^{-2} when grown on the Si substrate [15]. Numerous approaches have been used to solve these problems, such as special surface treatment [16], strained superlattices [17,18], low-temperature buffers [19] and growth on patterned substrates [20].

The first quantum dot (QD) laser monolithically grown on Si was reported in 1999 with its peak emission at 1.013 µm [21]. In 2011, Liu et al., achieved the first electrically pumped 1.3 µm InAs QD laser grow directly on Si substrate [22]. Since then, numerous approaches have been investigated to improve device performance. In 2017, Kryzhanovskaya et al., succeeded in demonstrating the first Si-based micro-disk lasers with minima Jth of 600 A/cm and emission covering 1320–1350 nm [23]. In 2018, an electronically pumped distributed feedback (DFB) laser array on Si substrate was realized, which could lase at room temperature with threshold current as low as 12 mA [24]. In 2019, Bowers et al., achieved the first tunable QD single-wavelength laser with 16 nm tuning range directly grown on Si under continue wave (CW) electrical injection at room temperature [25].

Although a lot of progress has been made in the epitaxial III-V light sources, much effort is needed to make this technology affordable for high volume, high-performance photonic integrated circuits (PICs), such as fewer defects, lower thresholds, higher temperature stability and uniformity. Additionally, low-loss active–passive coupling schemes need to be developed to integrate with other silicon-based components [26].

1.2. Heterogeneous III-V Light Sources

Heterogeneous integration is the process which combines III-V devices with silicon-based optoelectronic devices via wafer-bonding, including direct bonding, molecular bonding, metal bonding and polymer bonding [27,28]. Compared with direct epitaxial growth, heterogeneous integration is more versatile and flexible to integrate different materials from the perspective of the materials system, size, and processing simplicity.

In 2005, Bowers et al., demonstrated the first optically pumped heterogeneous laser on Si [29]. One year later, the research group realized the first electrically pumped heterogeneous laser [30]. Since then, the performance of heterogeneously integrated III-V on silicon components has continuously improved over the past decade. In 2015, Santis et al., realized a heterogeneous InP laser with sub-kHz quantum noise-limited linewidth [31]. In 2020, Thiessen et al., achieved a heterogeneously integrated InP DFB laser with threshold currents as low as 32 mA [32]. Heterogeneous integrated light sources have been used in commercial products by Intel since 2016. In 2020, a 400 Gbps PAM-4 fully integrated DR4 silicon photonics transmitter with four heterogeneously integrated DFB lasers has been demonstrated for data center applications [33].

Heterogeneous III-V light source has since developed rapidly in recent years due to the improved fabrication processes. However, it is limited by the complicated fabrication procedures, smaller yields, and incompatibility with traditional CMOS production line. For wider application in the future, the processing technology still needs to be further improved, and the processing cost needs to be reduced.

1.3. Er-Based Light Sources

Compared with the III-V light sources, rare earth element based light sources have better CMOS technology compatibility, which may have more potentials in monolithic integration application. Among them, the spontaneous emission of erbium ions (Er^{3+}) covers 1524–1574 nm, thulium ions (Tm^{3+}) covers 1680–2020 nm, holmium ions (Ho^{3+}) covers 1930–2130 nm [34–36]. For the on-chip optical communication at C band (1525–1565 nm), Er^{3+} is more suitable, with the advantages of long luminescence lifetime, small noise, and low process manufacturing cost. Consequently, Er-based materials have inspired significant research to silicon-based on-chip light sources, especially since the erbium-doped waveguide amplifier (EDWA) was first realized in 1985 [37]. For the compact size integration requirements, the Er^{3+} concentration of on-chip Er-based light sources need to be more than two orders higher than EDFA [38]. Therefore, it is crucial to choose the proper host materials.

In 2017, Ning et al., achieved giant optical gain in a single-crystal Er chloride silicate nanowire with Er concentration up to 1.62×10^{22} cm^{-3} [39]. A net material gain over 100 dB·cm^{-1} at wavelengths at approximately 1530 nm is possible due to the nanowire's single-crystalline material quality and its high Er concentration. In 2019, Sun et al. realized an Al_2O_3:Er slot waveguide amplifier by atomic layer deposition (ALD) [40]. By combining low-loss silicon nitride waveguides with high-quality Al_2O_3:Er films, up to 20 dB/cm net modal gain was achieved. In 2022, Kippenberg et al. demonstrated over 145 mW on-chip output power and >30 dB of small-signal gain based on Si_3N_4:Er, which greatly expands the application prospects of the Si_3N_4 platform [41].

With the broadening of the selection of host materials and the progress of fabrication technology, Er-based light sources have developed rapidly in recent years. Based on the advantages above, the application prospects of on-chip Er-based light sources are broader and more conducive to the future development of the silicon photonics industry.

In this paper, the recent progress and the state of the art in on-chip Er-based light sources are reviewed. We begin with comprehensive theoretical analysis of Er^{3+} luminescence model, followed by recent advances in on-chip Er-based light sources of different host materials. The advantages and disadvantages of different host materials are compared and analyzed. Finally, the future directions and existing challenges towards higher-level integration are discussed.

2. Electronic Energy Level Structure and Amplification in Er-Based Medium

The neutral form of the rare earth element Er is $[Xe]4f^{12}6s^2$, which has a similar electronic structure to xenon (Xe). The $6s^2$ electrons and the 4f electron, which are in a weakly bound state, are usually removed when bound into the host materials and becomes Er^{3+}. On this account, the partially filled 4f electron shell is shielded by the larger-radius 5s and 5p orbitals and forms a localized electronic environment. Therefore, the luminescence properties of Er^{3+} are almost unaffected by the host materials.

The energy-level model of Er^{3+} and the corresponding electronic transitions are shown in Figure 1, which contains ground state absorption (GSA), excited state absorption (ESA), spontaneous emission, stimulated emission, energy-transfer-upconversion (ETU) process and cross-relaxation (CR) process [38]. For Er-based amplifiers and lasers operating around C-band, the transition process is mainly based on $^4I_{13/2}$-$^4I_{15/2}$ stimulated emission, which can be pumped by 980 nm or 1480 nm lasers. Meanwhile, the spontaneous emission based on the $^4I_{13/2}$-$^4I_{15/2}$ transition would radiate non-coherent photons in a broad spectrum around the signal wavelength, which is known as amplified spontaneous emission (ASE) noise.

For Er-based optical amplifier, the expression for the gain coefficient g can be simplified as follows:

$$g(h\upsilon) = \sigma_{em}(h\upsilon)N_2 - \sigma_{abs}(h\upsilon)N_1, \tag{1}$$

where h is Planck constant, υ is the optical frequency, σ_{em} is the emission cross section, σ_{abs} is the absorption cross section, N_2 and N_1 are the concentration of Er^{3+} in the excited

(^{4}I$_{13/2}$) and ground (^{4}I$_{15/2}$) energy levels, respectively. σ_{em} and σ_{abs} are usually on the same order of magnitude. Therefore, to achieve optical net gain, N_2 need to be much higher than N_1, which can be achieved by pump absorption. The concentration of Er^{3+} in each energy level can be derived by rate equations [42].
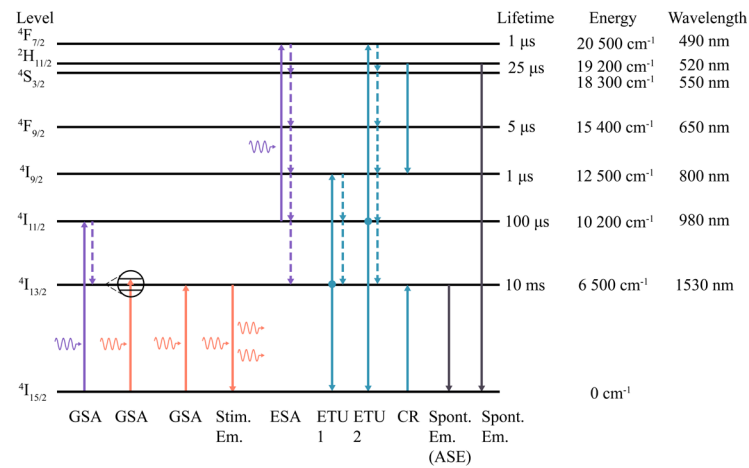

Figure 1. The energy-level model of Er^{3+}.

When signal light propagates in the gain medium, the internal signal-optical gain G can be expressed as:

$$G = \exp[(\Gamma g - \alpha)L], \tag{2}$$

where Γ is the optical mode confinement factor, α is the propagation loss and L is propagation length.

Small size and high gain are important performance parameters of silicon-based on-chip erbium-based light sources. From the above equations, it can be seen that in order to improve the signal gain (G) of the amplifier at a compact size, it is necessary to increase the Er^{3+} concentration (N) in the gain material, improve the optical mode confinement factor (Γ), and reduce the propagation loss (α). For on-chip Er-based light sources, the enhancement of Er^{3+} concentration is the most crucial, which is determined by the host material.

3. Gain Medium Based on Different Host Materials

3.1. Er-Doped Al$_2$O$_3$

Among the host materials, Al$_2$O$_3$ is of particular interest due to its numerous advantages. The transmission loss of Al$_2$O$_3$ is low over a wide wavelength range (1–6 μm). In addition, the binding sites of Al$_2$O$_3$ and Er^{3+} are well matched, which can increase the solubility of Er^{3+} and reduce the possibility of clustering. Therefore, the doping concentration of Er^{3+} in Al$_2$O$_3$ is approximately 2~3 orders of magnitude higher than that in EDFA, which is beneficial to achieve high gain in a compact device size. In 1993, Hoven et al. demonstrated the first successful incorporation of optically active Er in Al$_2$O$_3$ films by ion implantation [43]. Since then, several approaches have been taken to improve photoluminescence performance of Al$_2$O$_3$:Er [44].

In 2014, Watts' research group deposited Al$_2$O$_3$:Er layers by co-sputtering in an oxygen-rich environment [45]. The background loss and dopant concentration in the Al$_2$O$_3$:Er film were <0.1 dB/cm and 0.9×10^{20} cm^{-3}, respectively. Based on this gain medium, a DFB hybrid waveguide laser was designed. The Si$_3$N$_4$ film was patterned to form DFB grating structure for the reason that Al$_2$O$_3$ is hard to etch. The confinement factor in the gain medium is 83% and the pump–signal overlap factor is 90%. Therefore, the pump and signal light can be well confined in the gain medium, which is beneficial to improve the conversion efficiency of the on-chip waveguide amplifier. A maximum output power of 75 mW was experimentally demonstrated without any thermal damage. Since then, the research group designed several on-chip waveguide lasers with different structures

and an improvement of 1.8 times in the lasing efficiency was achieved by optimizing the waveguide laser structure [46–48].

In order to further improve the luminescence properties of the Al_2O_3:Er thin film and reduce the propagation loss, Sun's research group prepared Al_2O_3:Er thin films by ALD process in 2019 [40]. Si_3N_4 was etched to form the slot waveguide structure so that the optical field can be better confined in the intermediate gain medium, as shown in Figure 2a. Al_2O_3:Er thin films were deposited through layer-by-layer sequence and repeated multiple times on Si_3N_4 slot waveguides, as shown in Figure 2b. The optical mode of TE and TM in the slot waveguide are shown in Figure 2c,d, respectively, which illustrates that the optical modes are well confined in the gain medium inside the slot waveguide. Finally, up to ~20.1 ± 7.31 dB/cm net modal gain and at least ~52.4 ± 13.8 dB/cm net material gain was experimentally observed in the sub-mm long hybrid Al_2O_3:Er–Si_3N_4 slot waveguides.
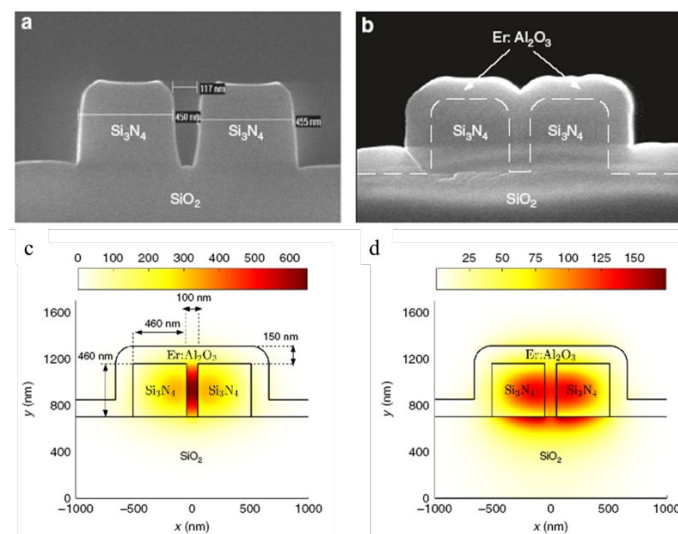
Figure 2. (**a**) The cross-section of the fabricated Si_3N_4 slot waveguide. (**b**) The cross-section of the Al_2O_3:Er–Si_3N_4 hybrid slot waveguide. (**c**) The TE and (**d**) TM optical mode distribution at 1533 nm in the hybrid slot waveguides [40].

Although the hybrid Al_2O_3:Er–Si_3N_4 waveguide structures have made great progress and achieve high on-chip optical gain, it is hard to couple and integrate with other on-chip optoelectronic devices. In order to solve this problem and further confine the optical mode in the gain medium, Mu et al. achieved high-gain on-chip waveguide amplifiers via double-layer monolithic integration technology [49]. The Al_2O_3:Er and the Si_3N_4 waveguides are located in two individual layers which are separated by a thin SiO_2 film. Thus, the structure parameters of the Al_2O_3:Er and the Si_3N_4 waveguides can be optimized, respectively, and the pump and signal light can be better confined in the gain medium, which is conductive to improve the conversion efficiency of pump light. Meanwhile, the mode transfer between the two layers is achieved by a vertically tapered adiabatic coupler and the optical mode is efficiently coupled from the Si_3N_4 waveguide to the Al_2O_3:Er waveguide. Finally, up to 18.1 ± 0.9 dB net gain was achieved at 1532 nm with an over 70 nm broadband gain covering S, C, and L bands.

3.2. Er Silicate

For Er-doped gain mediums, the maximum material gains are limited by the solubility of Er^{3+} in the host materials. In contrast, Er^{3+} exists as compound cation in Er silicate. For this reason, the concentration of Er^{3+} is not limited by the solid solubility and can reach up to 10^{22} cm^{-3}, which is two orders higher than other Er doped gain mediums [50]. Moreover, by introducing yttrium (Y) or ytterbium (Yb) into Er silicate, the concentration quenching effect caused by high Er^{3+} concentration can be effectively suppressed and the absorption efficiency of pump light can be improved, thus the optical gain of Er silicate can

be future improved [51–55]. In 2004, Isshiki et al., first fabricated Er silicate compounds (Er_2SiO_5) by a wet chemical method using $ErCl_3$ deposited on Si substrates and the photo-luminescence (PL) was observed at approximately 1.53 μm at room temperature [56]. Then, Priolo's group fabricated Er silicate by radio frequency magnetron sputtering and oxygen annealing is proved to remove defects efficiently and the PL intensity can be strongly enhanced [57,58]. Wang's research group demonstrated that the introduction of bismuth can effectively reduce the annealing temperature required for Er silicate crystallization [59].

In 2017, Ning et al., demonstrated a giant net material gain of waveguide amplifier, which is benefits from the high material quality and high Er^{3+} concentration of the single-crystal Er chloride silicate nanowire [39]. The experimental measurement is shown in Figure 3a. The backward pumping scheme was adopted, which can improve the utilization of the pump light and enhance the signal gain. The silicate nanowire was end-butt coupled to the taper fibers, as shown in Figure 3b,c and the coupling efficiency is on the order of 10–15%. Finally, a net material gain over 100 dB·cm^{-1} at 1530 nm was achieved.
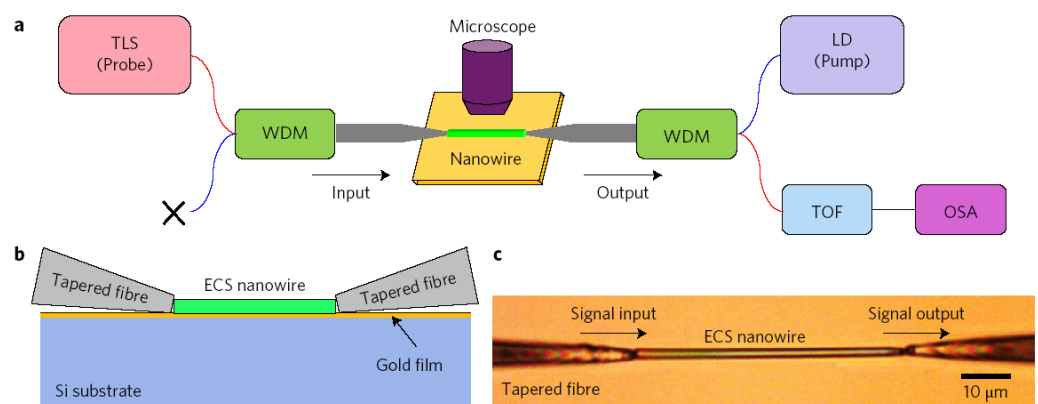

Figure 3. Experimental layout of the signal enhancement measurement. (**a**) Schematic of the pump-probe measurement. (**b**) Side view of the coupling configuration. The tapered fibers are placed in direct contact with the two end-facets of the nanowire at a small angle. (**c**) Top-view microscope image of the coupling system [39].

Although over 100 dB·cm^{-1} material gain has been realized, the fabrication of Er chloride silicate nanowire is complicated, the cross-section is small and coupling efficiency is low, thus it is hard to integrate with other on-chip devices. To solve this problem, Wang's research group have done a lot of work to achieve on-chip waveguide amplifiers and lasers based on Er silicate gain medium [59–65]. For the reason that Er silicate is hard to etch, some hybrid waveguide structures combining different materials are adopted to avoid etch Er silicate and the performance of the devices are optimized.

For strip-loaded waveguide amplifier, as shown in Figure 4a, the SiO_2 film was deposited on the Er/Yb silicate film and etched into strip waveguide structure [60]. The optical mode of the signal light is shown in the inset and it can be well confined in the gain medium. Although the propagation loss is large, a 5.5 dB signal enhancement was observed when the pump power is 372 mW.

For hybrid waveguide amplifier, as shown in Figure 4b, the Si_3N_4 was etched into strip waveguide structure and then Er/Yb silicate was deposited on it [61]. Although the confinement factor of the signal light in the gain medium is small, the propagation loss could be greatly reduced due to the high quality of the Si_3N_4 waveguide. Finally, up to 5.5 dB/cm and 10.1 dB/cm signal enhancement was achieved when the annealing temperature was 750 °C and 1000 °C, respectively, which proved that the PL characters of Er silicate films is higher when the annealing temperature is higher.
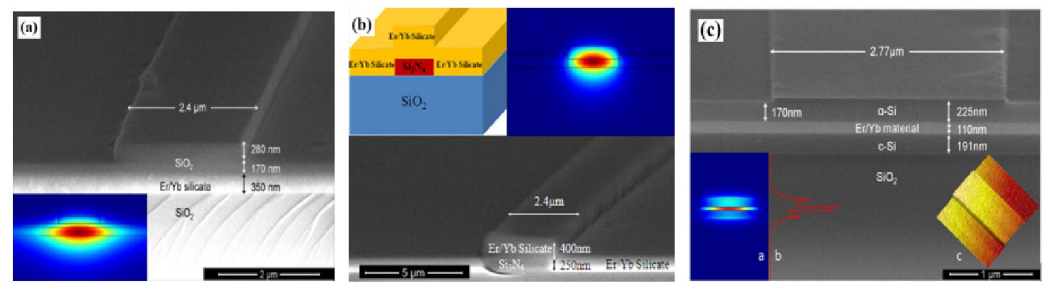
Figure 4. Scanning electron microscope (SEM) of (**a**) strip loaded waveguide amplifier, (**b**) hybrid waveguide amplifier, (**c**) slot waveguide amplifier [42].

For slot waveguide structure, as shown in Figure 4c, the Er/Yb silicate film was deposited on the Si film and after that, poly-Si was deposited and etched into strip waveguide [62]. The TM mode of the optical filed could be well confined in the gain medium in the slot due to the continuity of normal electric displacement at the interface. Therefore, the overlap factor of pump and signal light in the gain medium was high, which is beneficial to improve the conversion efficiency of the pump light and the optical gain of the waveguide amplifier. Finally, a 1.7 dB signal enhancement was observed at 1.53 μm.

Based on the above gain medium, the research group designed a silicon-based on-chip waveguide laser of sub-kHz narrow linewidth and high output power, as shown in Figure 5a [63]. The resonant cavity of the waveguide laser consists DFB cavity, pump-resonant external distributed Bragg reflector (DBR) cavity, signal-resonant external DFB cavity. The DFB cavity is used to obtain lasing at 1535 nm, the pump-resonant external DBR cavity is used to improve pump absorption efficiency and the signal-resonant external DFB cavity is used to provide additional optical feedback. Based on the above structure, the output power and efficiency of the laser can be improved, and the threshold and linewidth of the laser can be reduced. In addition, the Si_3N_4 films are added to reduce the propagation loss of the waveguide laser, as shown in Figure 5b. Over 90 mW saturated output power is achieved at 1535 nm with a maximum power conversion efficiency of 66%. The threshold of the waveguide laser is 22 mW and the linewidth is approximately 755 Hz.
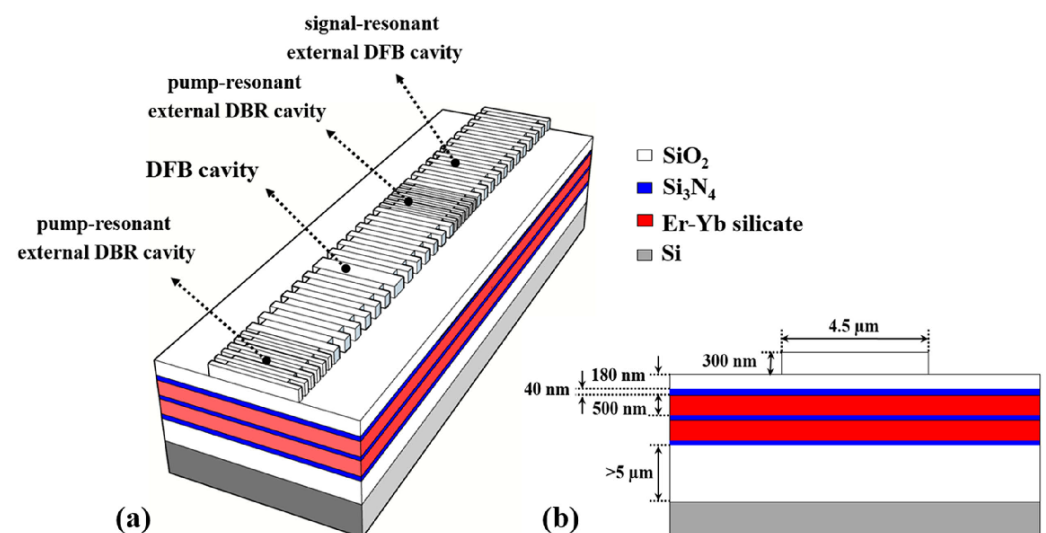
**Figure 5.** The 3D scheme diagram (**a**) and the cross section (**b**) of the silicon-based on-chip waveguide laser [63].

3.3. Other Er-Doped Host Material

Lithium niobate on insulator (LNOI) is a promising material platform for the photonic integrated circuit, due to its broad optical transparency window, high refractive index, high nonlinear coefficient, and large electro-optical effect [66,67]. So far, numerous LNOI-based

devices have been achieved and commercialized, such as electro-optic modulators and nonlinear optical devices [68–73]. Recently, LNOI:Er has attracted great attention due to the high Er doping concentration and low propagation loss [74].

In 2021, Wu et al., achieved a single-frequency laser based on LNOI:Er by introducing mode-dependent loss and gain competition, as shown in Figure 6a [75]. The radius of the microring is 105 µm, which corresponds to the free spectrum range (FSR) of 192 GHz. The gap between the microring and the bus waveguide is 700 nm, as shown in Figure 6b and the cross section of the waveguide is shown in Figure 6c. There are four modes supported in this structure, containing TE_{00}, TE_{10}, TM_{00}, and TM_{10}, as shown in Figure 6d. The overlap of TE_{10}, TM_{00}, and TM_{10} with the rough sidewall is lager than that of TE_{00}, thus the scattering loss is higher. Considering the gain competition of the microring laser, only the TE_{00} mode could exit and lase. Finally, an output power of 2.1 µW was achieved, with a side-mode suppression of 35.5 dB, and a linewidth of 0.9 MHz. One year later, the research group demonstrated a LNOI:Er thin film waveguide amplifier [76]. The 600 nm-thick LNOI:Er thin film is transferred to the substrate and etched off 410 nm to form the ridge waveguide structure with chromium (Cr) as hard mask. The PL lifetime at 1530 nm is 2.3 ms. Up to 27.94 dB signal enhancement, 16.0 dB internal net gain (6.20 dB/cm), 8.84 dBm saturation power, 4.59 dB/mW power conversion efficiency has been achieved with 4.49 dB noise figure when the waveguide amplifier is 2.58-cm long.
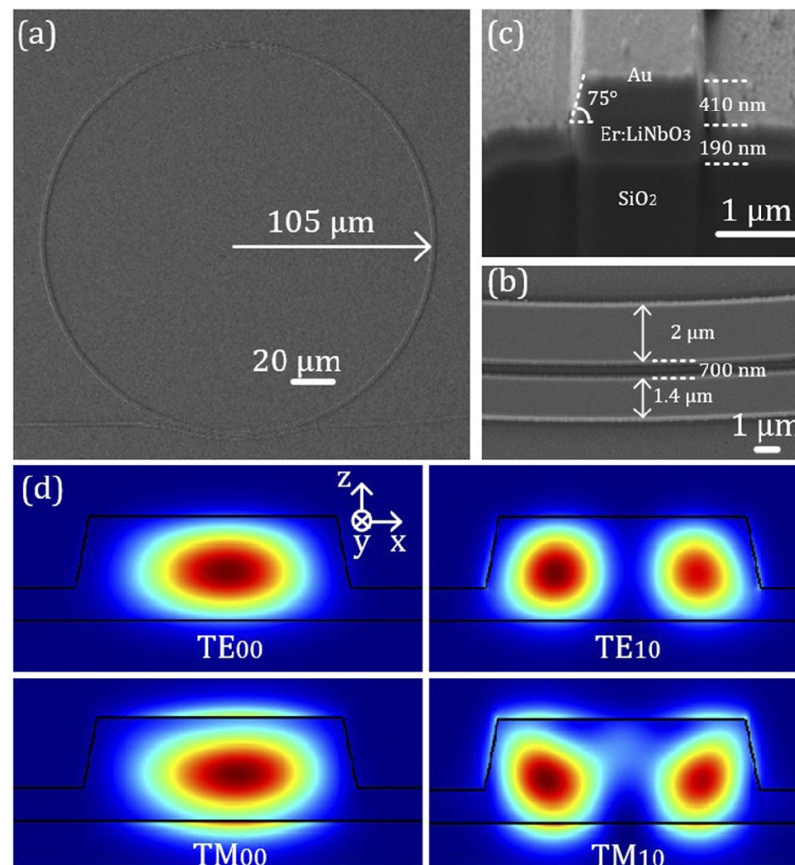
Figure 6. The SEM image of (**a**) the microring, (**b**) the pulley coupling region and (**c**) the end facet. (**d**) The four modes supported in the microring waveguide [75].

Compared to other host materials, Si_3N_4 has several advantages including a wider transparency window [77], ultra-low two-photon absorption effect at telecom wavelengths, and low propagation losses of <3 dB/m [78]. These properties have made Si_3N_4 a widely used platform in silicon integrated photonic applications [79,80]. In 2022, Kippenberg et al. demonstrated an ultra-high gain Er-doped Si_3N_4 amplifier, as shown in Figure 7a [41].

The main fabrication processes are shown in Figure 7b,c, containing photonic damascene process and ion implantation. The length of the waveguide amplifier is 0.5 m and the propagation loss is less than 5 dB/m, as shown in Figure 7d. The waveguide amplifier was butt-end coupled and green luminescence from cooperative upconversion was observed, as shown in Figure 7e. The calculated Er concentration, calculated optical mode intensity and measured concentration by Rutherford backscattering spectrometry (RBS) are shown in Figure 7f. The propagation loss of the waveguide increased sharply after ion implantation and decreased after annealing at 1000 °C in oxygen for 1 h, as shown in Figure 7g. Over 145 mW on-chip output power and over 30 dB of small-signal gain have been observed, which achieved giant progress in the field of silicon-based on-chip light sources.
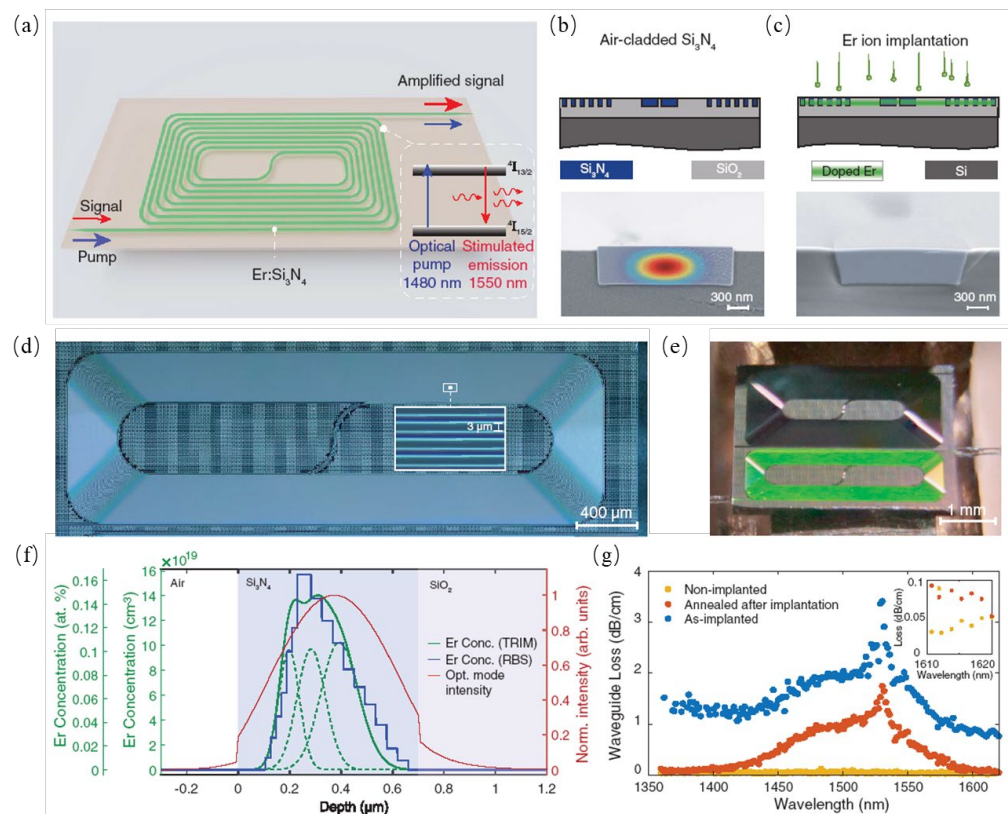
Figure 7. (**a**) The structure of the Si_3N_4:Er waveguide amplifier. (**b**) The damascene process and the optical mode in the waveguide. (**c**) The ion implantation process. (**d**) The optical image of the 0.5 m long waveguide. (**e**) The waveguide amplifier butt-end coupled with fibers (**f**) The calculated Er concentration (green), simulated optical mode (red) and measured concentration (blue) by RBS. (**g**) Measured propagation losses before ion implantation, as-implanted, and after annealing [41]. Reprinted/adapted with permission from Ref. [41]. 2022, The American Association for the Advancement of Science.

4. Discussion

Table 1 summarized the experimental results of representative on-chip Er-based waveguide amplifiers. The propagation loss of Al_2O_3:Er is relatively low and the gain performance is affected by the preparation method. Prepared by magnetron sputtering, the process is simple and the uniformity is good, but the optical gain is relatively low. On the contrary, the optical gain is much higher when prepared by ALD, but the process is complicated and the growth rate is low; Benefit from the single-crystalline structure and the high Er concentration, a net material gain over 100 dB·cm^{-1} have been achieved by Er chloride silicate nanowire. However, it is too hard to fabricate and integrate with other on-chip devices; As a new host material, LN has the characteristics of high nonlinear coefficient and high refractive index, and has been widely used in on-chip modulators. The optical

gain of LNOI:Er is high, but currently Er^{3+} are difficult to dope and the propagation loss is still large; Si_3N_4:Er has ultra-low propagation loss, hence a 0.5 m long on-chip waveguide amplifier could be fabricated and over 145 mW on-chip output power was realized, which achieved giant progress in the field of silicon-based on-chip light sources.

Table 1. Comparison for representative on-chip Er-based waveguide amplifiers.

Host Material	Signal Wavelength	Pump Wavelength	Waveguide Length	Internal Net Gain	Propagation Loss	Refs.
Al_2O_3	1533 nm	977 nm	5.4 cm	2 dB/cm	0.3 dB/cm	[44]
Al_2O_3	1533 nm	1470 nm	250 µm	20.1 dB/cm	0.62 dB/cm	[40]
Al_2O_3	1532 nm	980 nm	10 cm	1.81 dB/cm	0.64 dB/cm	[49]
Silicate	1532 nm	980 nm	56.2 µm	122 dB/cm	~	[39]
LN	1532 nm	980 nm	10 cm	2 dB/cm	0.72 dB/cm	[74]
LN	1531.6 nm	1484 nm	2.58 cm	6.2 dB/cm	2.5 dB/cm	[76]
Si_3N_4	1562 nm	1480 nm	0.5 m	0.6 dB/cm	0.05 dB/cm	[41]

In summary, the key issues for achieving the on-chip Er-based light sources are compact size, high gain and low loss. In order to meet the above requirements and satisfy the application requirements of on-chip integration, the following aspects can be considered, including the choice of gain mediums, the optimization of waveguide amplifier structures, and the design for resonator structures of the waveguide laser.

The choice of gain medium is crucial. The selection of host materials determines the upper limit of the erbium ion concentration in the gain medium, as well as the maximum material gain that can be achieved. Although too high erbium ion concentration will lead to concentration quenching effect, it can be optimized by introducing Yb and Y [53]. The preparation method of gain medium is also important. The film transfer method is difficult to achieve large-scale integration with other on-chip optoelectronic devices. ALD process can achieve high-quality gain mediums, but the steps are complicated and the growth rate is slow, so that the cost is too high to meet the needs for large-scale integration. Magnetron sputtering can achieve low-cost, large-scale fabrication, but the propagation loss in the gain medium is large. How to further improve the quality of the gain medium prepared by magnetron sputtering and reduce the transmission loss is an important direction for the future development. Chemical vapor deposition (CVD) seems a compromise method, combing the advantages of low preparation cost and high film quality, which is widely used in various aspects.

The structure of the on-chip waveguide amplifier should be optimized. For the waveguide amplifiers with strip or ridge waveguide structures, the propagation loss is mainly determined by the sidewall roughness, which can be effectively reduced by adopting wide waveguide structures and improving the etching process. For the hybrid waveguide structures which combine with other materials, such Si_3N_4, the etching of the gain medium can be avoided and the transmission loss can be effectively reduced. However, the confinement factor in the gain medium is relatively low, which would reduce the gain of the waveguide amplifier. In addition, the coupler structure of the waveguide amplifier with the traditional Si waveguide needs to be considered and optimized. In addition, the optimal length of waveguide amplifier is associated with the Er^{3+} concentration and the maximum input on-chip pump power [42]. The signal gain would be attenuated if the pump power cannot achieve Er^{3+} population inversion over the entire length of the waveguide amplifier. Bi-directional pumping can also be considered to improve the net gain of the waveguide amplifier [76].

The resonant cavity structure of the on-chip waveguide laser should be improved. The pumping threshold of the waveguide amplifier can be reduced and the output power can be increased by adopting appropriate resonant cavity structures. At present, the microring resonator, DBR resonator and DFB resonator are the mainly used resonant cavity structures. However, most of the reported microring waveguide lasers operate under the condition

of multi-longitudinal modes. Although some methods have been adopted, the side mode suppression effect is still not good enough. Furthermore, limited by the compact size of the microring waveguide laser, the output power is relatively low, which is hard to meet the requirements for on-chip integrated waveguide lasers. On the other hand, combined with Bragg gratings, the DBR and DFB resonant cavity structures provide a good technical solution for realizing on-chip small-sized, high-gain waveguide lasers. Compared to DBR waveguide lasers, DFB waveguide lasers have better single-mode stability so that they are more widely adopted. In addition, the resonant cavity structures of the DFB waveguide lasers can be future optimized to improve the output power and the linewidth characteristics [63–65].

5. Conclusions

In consideration of the rapid development of silicon-based photonics technology and the increasing degree of on-chip integration, there is an urgent need for high-efficiency silicon-based on-chip light sources to solve the increasingly serious signal emitting and transmission problems. As an effective solution for on-chip light sources, Er-based light sources have the advantages of CMOS compatibility, ease of integration and lower cost. Therefore, the application prospects of on-chip Er-based light sources are broader and more conducive to the future development of the silicon photonics industry. The recent progress of on-chip Er-based light sources with different host materials is reviewed in this paper. With the continuous efforts of researchers from all over the world, these Er-based host materials have the great prospects for applications in scale-integrated on chip light sources, which can be widely used in silicon photonics platform.

Author Contributions: Conceptualization, B.W. and X.W.; investigation, B.W. and P.Z.; resources, X.W.; writing—original draft preparation, B.W., P.Z. and X.W.; writing—review and editing, B.W., P.Z. and X.W.; visualization, B.W., P.Z. and X.W.; supervision, X.W.; project administration, X.W.; funding acquisition, X.W. All authors have read and agreed to the published version of the manuscript.

Institutional Review Board Statement: Not applicable.

Informed Consent Statement: Not applicable.

Data Availability Statement: Not applicable.

Conflicts of Interest: The authors declare no conflict of interest.

References

1. Moore, G.E. Cramming more components onto integrated circuits. *Electronics* **1965**, *38*, 114–117. [CrossRef]
2. Waldrop, M.M. More than Moore. *Nature* **2016**, *530*, 145–147.
3. Soref, R.A. Silicon-based optoelectronics. *Proc. IEEE* **1993**, *81*, 1687–1706. [CrossRef]
4. Margalit, N.; Xiang, C.; Bowers, S.M.; Bjorlin, A.; Blum, R.; Bowers, J.E. Perspective on the future of silicon photonics and electronics. *Appl. Phys. Lett.* **2021**, *118*, 220501. [CrossRef]
5. Bogaerts, W.; Perez, D.; Capmany, J.; Miller, D.; Poon, J.; Englund, D.; Morichetti, F.; Melloni, A. Programmable photonic circuits. *Nature* **2020**, *586*, 207–216. [CrossRef] [PubMed]
6. Bai, B.; Shu, H.; Wang, X.; Zou, W. Towards silicon photonic neural networks for artificial intelligence Sci. *China Inform. Sci.* **2020**, *63*, 160403. [CrossRef]
7. Teklu, B.; Bina, M.; Paris, M.G.A. Noisy propagation of Gaussian states in optical media with finite bandwidth. *Sci. Rep.* **2022**, *12*, 11646. [CrossRef]
8. Teklu, B. Continuous-variable entanglement dynamics in Lorentzian environment. *Phys. Lett. A* **2022**, *432*, 128022. [CrossRef]
9. Shen, B.; Shu, H.; Zhou, L.; Wang, X. A design method for high fabrication tolerance integrated optical mode multiplexer. *Sci. China Inform. Sci.* **2020**, *63*, 160409. [CrossRef]
10. Reed, G.T.; Mashanovich, G.; Gardes, F.Y.; Thomson, D.J. Silicon optical modulators. *Nat. Photonics* **2010**, *4*, 518–526. [CrossRef]
11. Michel, J.; Liu, J.L.; Kimerling, L.C. High-performance Ge-on-Si photodetectors. *Nat. Photonics* **2010**, *4*, 527–534. [CrossRef]

12. Shu, H.; Chang, L.; Tao, Y.; Shen, B.; Xie, W.; Jin, M.; Netherton, A.; Tao, Z.; Zhang, X.; Chen, R.; et al. Microcomb-driven silicon photonic systems. *Nature* **2022**, *605*, 457–463. [CrossRef] [PubMed]

13. Morichetti, F.; Milanizadeh, M.; Petrini, M.; Zanetto, F.; Ferrari, G.; Aguiar, D.O.; Guglielmi, E.; Sampietro, M.; Meiioni, A. Polarization-transparent silicon photonic add-drop multiplexer with wideband hitless tuneability. *Nat. Commun.* **2021**, *12*, 4324. [CrossRef] [PubMed]

14. Liang, D.; Bowers, J.E. Recent progress in lasers on silicon. *Nat. Photonics* **2010**, *4*, 511–517. [CrossRef]

15. Kawanami, H. Heteroepitaxial technologies of III–V on Si. *Sol. Energy Mater. Sol. C* **2001**, *66*, 479–486. [CrossRef]

16. Xie, Y.H.; Wang, K.L.; Kao, Y.C. An investigation on surface conditions for Si molecular beam epitaxial (MBE) growth. *J. Vac. Sci. Technol. A* **1985**, *3*, 1035. [CrossRef]

17. Samonji, K.; Yonezu, H.; Takagi, Y.; Iwaki, K.; Ohshima, N.; Shin, J.K.; Pak, K. Reduction of threading dislocation density in InP-on-Si heteroepitaxy with strained short-period superlattices. *Appl. Phys. Lett.* **1996**, *69*, 100–102. [CrossRef]

18. Yamaguchi, M.; Sugo, M.; Itoh, Y. Misfit stress dependence of dislocation density reduction in GaAs films on Si substrates grown by strained-layer superlattices. *Appl. Phys. Lett.* **1989**, *54*, 2568–2570. [CrossRef]

19. Nozawa, K.; Horikoshi, Y. Low threading dislocation density GaAs on Si(100) with InGaAs/GaAs strained-layer superlattice grown by migration-enhanced epitaxy. *Jpn. J. Appl. Phys.* **1991**, *30*, 668–671. [CrossRef]

20. Yamaichi, E.; Ueda, T.; Gao, Q.; Yamagishi, C.; Akiyama, M. Method to obtain low-dislocation-density regions by patterning with SiO_2 on GaAs/Si followed by annealing. *Jpn. J. Appl. Phys.* **1994**, *33*, 1442–1444. [CrossRef]

21. Linder, K.K.; Phillips, J.; Qasaimeh, O.; Liu, X.F.; Krishna, S.; Bhattacharya, P. Self-organized $In_{0.4}Ga_{0.6}As$ quantum-dot lasers grown on Si substrates. *Appl. Phys. Lett.* **1999**, *74*, 1355. [CrossRef]

22. Wang, T.; Liu, H.; Lee, A.; Pozzi, F.; Seeds, A. 1.3-μm InAs/GaAs quantum-dot lasers monolithically grown on Si substrates. *Opt. Express* **2011**, *19*, 11381–11386. [CrossRef] [PubMed]

23. Kryzhanovskaya, N.; Moiseev, E.; Polubavkina, Y.; Maximov, M.; Kulagina, M.; Troshkov, S.; Zadiranov, Y.; Guseva, Y.; Lipovskii, A.; Tang, M.; et al. Heat-sink free CW operation of injection microdisk lasers grown on Si substrate with emission wavelength beyond 1.3 μm. *Opt. Lett.* **2017**, *42*, 3319–3322. [CrossRef] [PubMed]

24. Wang, Y.; Chen, S.; Yu, Y.; Zhou, L.; Liu, L.; Yang, C.; Liao, M.; Tang, M.; Liu, Z.; Wu, J.; et al. Monolithic quantum-dot distributed feedback laser array on silicon. *Optica* **2018**, *5*, 528–533. [CrossRef]

25. Wan, Y.; Zhang, S.; Norman, J.C.; Kennedy, M.J.; He, W.; Liu, S.; Xiang, C.; Shang, C.; He, J.J.; Gossard, A.C.; et al. Tunable quantum dot lasers grown directly on silicon. *Optica* **2019**, *6*, 1394–1400. [CrossRef]

26. Wang, Y.; Norman, J.; Liu, S.; Liu, A.; Bowers, J.E. Quantum dot lasers and amplifiers on silicon: Recent advances and future developments. *IEEE Nanotechnol. Mag.* **2021**, *15*, 8–22.

27. Liang, D.; Bowers, J.E. Recent progress in heterogeneous III-V-on-silicon photonic integration. *Light Adv. Manuf.* **2021**, *2*, 5. [CrossRef]

28. Bao, S.; Wang, Y.; Lina, K.; Zhang, L.; Wang, B.; Sasangka, W.A.; Lee, K.E.K.; Chua, S.J.; Michel, J.; Fitzgerald, E.; et al. A review of silicon-based wafer bonding processes, an approach to realize the monolithic integration of Si-CMOS and III–V-on-Si wafers. *J. Semicond.* **2021**, *42*, 023106. [CrossRef]

29. Park, H.; Fang, A.W.; Kodama, S.; Bowers, J.E. Hybrid silicon evanescent laser fabricated with a silicon waveguide and III-V offset quantum wells. *Opt. Express* **2005**, *13*, 9460–9464. [CrossRef]

30. Fang, A.W.; Park, H.; Cohen, O.; Jones, R.; Paniccia, M.J.; Bowers, J.E. Electrically pumped hybrid AlGaInAs-silicon evanescent laser. *Opt. Express* **2006**, *14*, 9203–9210. [CrossRef]

31. Santis, C.T.; Vilenchik, Y.; Yariv, A.; Satyan, N.; Rakulijic, G. Sub-kHz quantum linewidth semiconductor laser on silicon chip. In Proceedings of the 2015 Conference on Lasers and Electro-Optics (CLEO), San Jose, CA, USA, 10–15 May 2015; pp. 1–2.

32. Thiessen, T.; Mak, J.C.C.; Fonseca, J.D.; Ribaud, K.; Jany, C.; Poon, J.K.S.; Menezo, S. Back-side-on-BOX heterogeneously integrated III-V-on-silicon O-band distributed feedback lasers. *J. Lightwave Technol.* **2020**, *38*, 3000–3006. [CrossRef]

33. Yu, H.; Doussiere, P.; Patel, D.; Lin, W.; Hemyari, K.; Park, J.; Jan, C.; Herrick, R.; Hoshino, I.; Busselle, L.; et al. 400Gbps Fully Integrated DR4 Silicon Photonics Transmitter for Data Center Applications. In Proceedings of the 2020 Optical Fiber Communications Conference and Exhibition (OFC), San Diego, CA, USA, 8–12 March 2020. paper T3H.6.

34. Li, N.; Su, Z.; Magden, E.S.; Callahan, P.T.; Shtyrkova, K.; Xin, M.; Ruocco, A.; Baiocco, C.; Ippen, E.P.; Kartner, F.X.; et al. High-power thulium lasers on a silicon photonics platform. *Opt. Lett.* **2017**, *42*, 1181–1184. [CrossRef] [PubMed]

35. Li, N.; Magden, E.S.; Su, Z.; Singh, N.; Ruocco, A.; Xin, M.; Byrd, M.; Callahan, P.T.; Bradley, J.D.B.; Baiocco, C.; et al. Broadband 2-μm emission on silicon chips: Monolithically integrated Holmium lasers. *Opt. Express* **2018**, *26*, 2220–2230. [CrossRef] [PubMed]

36. Li, N.; Vermeulen, D.; Su, Z.; Magden, E.S.; Xin, M.; Singh, N.; Ruocco, A.; Notaros, J.; Poulton, C.V.; Timurdogan, E.; et al. Monolithically integrated Er-doped tunable laser on a CMOS-compatible silicon photonics platform. *Opt. Express* **2018**, *26*, 16200–16211. [CrossRef] [PubMed]

37. Poole, S.B.; Payne, D.N.; Fermann, M.E. Fabrication of low-loss optical fibers containing rare-earth ions. *Electron. Lett.* **1985**, *21*, 737–738. [CrossRef]

38. Bradley, J.D.B.; Pollnau, M. Erbium-doped integrated waveguide amplifiers and lasers. *Laser Photonics Rev.* **2011**, *5*, 368–403. [CrossRef]

39. Sun, H.; Yin, L.; Liu, Z.; Zheng, Y.; Fan, F.; Zhao, S.; Feng, X.; Li, Y.; Ning, N.Z. Giant optical gain in a single-crystal erbium chloride silicate nanowire. *Nat. Photonics* **2017**, *11*, 589–593. [CrossRef]

40. Ronn, J.; Zhang, W.; Autere, A.; Leroux, X.; Pakarinen, L.; Alonso-Ramos, C.; Saynatjoki, A.; Lipsanen, H.; Vivien, L.; Cassan, E.; et al. Ultra-high on-chip optical gain in erbium-based hybrid slot waveguides. *Nat. Commun.* **2019**, *10*, 432. [CrossRef]

41. Liu, Y.; Qiu, Z.; Ji, X.; Lukashchuk, A.; He, J.; Riemensberger, J.; Hafermann, M.; Wang, R.N.; Liu, J.; Ronning, C.; et al. A photonic integrated circuit–based erbium-doped amplifier. *Sciences* **2022**, *376*, 1309–1313. [CrossRef]

42. Wang, X.; Zhou, P.; He, Y.; Zhou, Z. Erbium silicate compound optical waveguide amplifier and laser. *Opt. Mater. Express* **2018**, *8*, 2970–2990. [CrossRef]

43. Hoven, G.N.; Snoeks, E.; Polman, A.; Uffelen, J.W.M.; Oei, Y.S.; Smit, M.K. Photoluminescence characterization of Er-implanted Al_2O_3 films. *Appl. Phys. Lett.* **1993**, *62*, 3065. [CrossRef]

44. Bradley, J.D.B.; Agazzi, L.; Geskus, D.; Worhoff, A.K.; Pollnau, M. Gain bandwidth of 80 nm and 2 dB/cm peak gain in Al_2O_3:Er^{3+} optical amplifiers on silicon. *J. Opt. Soc. Am. B* **2010**, *27*, 187–196. [CrossRef]

45. Hosseini, E.S.; Bradley, J.D.B.; Sun, J.; Leake, G.; Adam, T.N.; Coolbaugh, D.D.; Watts, M.R. CMOS-compatible 75 mW Er-doped distributed feedback laser. *Opt. Lett.* **2014**, *39*, 3106–3109. [CrossRef] [PubMed]

46. Sun, J.; Hosseini, E.S.; Bradley, J.D.B.; Adam, T.N.; Leake, G.; Coolbaugh, D.; Watts, M.R. Uniformly spaced $\lambda/4$-shifted Bragg grating array with wafer-scale CMOS-compatible process. *Opt. Lett.* **2013**, *38*, 4002–4004. [CrossRef] [PubMed]

47. Bradley, J.D.B.; Hosseini, E.S.; Su, Z.; Adam, T.N.; Leake, G.; Coolbaugh, D.; Watts, M.R. Monolithic erbium- and ytterbium-doped microring lasers on silicon chips. *Opt. Express* **2014**, *22*, 12226–12237. [CrossRef]

48. Singh, G.; Bradley, J.D.B.; Li, N.; Magden, E.S.; Moresco, M.; Adam, T.N.; Leake, G.; Coolbaugh, D.; Watts, M.R. Resonant pumped Er-doped waveguide lasers using distributed Bragg reflector cavities. *Opt. Lett.* **2016**, *41*, 1189–1192. [CrossRef]

49. Mu, J.; Dijkstra, M.; Korterik, J.; Offerhaus, H.; Garcia-Blaco, S.M. High-gain waveguide amplifiers in Si_3N_4 technology via double-layer monolithic integration. *Photonics Res.* **2020**, *8*, 1634–1641. [CrossRef]

50. Wang, X.J.; Nakajima, T.; Isshiki, H.; Kimura, T. Fabrication and characterization of Er silicates on SiO_2/Si substrates. *Appl. Phys. Lett.* **2009**, *95*, 041906. [CrossRef]

51. Wang, X.J.; Wang, B.; Wang, L.; Guo, R.M.; Isshiki, H.; Kimura, T.; Zhou, Z. Extraordinary infrared photoluminescence efficiency of $Er_{0.1}Yb_{1.9}SiO_5$ films on SiO_2/Si substrates. *Appl. Phys. Lett.* **2011**, *98*, 071903. [CrossRef]

52. Wang, X.J.; Yuan, G.; Isshiki, H.; Kimura, T.; Zhou, Z. Photoluminescence enhancement and high gain amplification of $Er_xY_{2-x}SiO_5$ waveguide. *Appl. Phys. Lett.* **2010**, *108*, 013506. [CrossRef]

53. Cardile, P.; Miritello, M.; Priolo, F. Energy transfer mechanisms in Er-Yb-Y disilicate thin films. *Appl. Phys. Lett.* **2012**, *100*, 251913. [CrossRef]

54. Wang, B.; Guo, R.; Wang, X.; Wang, L.; Yin, B.; Zhou, Z. Large electroluminescence excitation cross section and strong potential gain of Er in ErYb silicate. *J. Appl. Phys.* **2013**, *113*, 103108. [CrossRef]

55. Zhou, P.; Wang, X.; He, Y.; Wu, Z.; Du, J.; Fu, E. Effect of deposition mechanisms on the infrared photoluminescence of erbium-ytterbium silicate films under different sputtering methods. *J. Appl. Phys.* **2019**, *125*, 175114. [CrossRef]

56. Isshiki, H.; Dood, M.J.A.; Polman, A.; Kimura, T. Self-assembled infrared-luminescent Er-Si-O crystallites on silicon. *Appl. Phys. Lett.* **2004**, *85*, 4343. [CrossRef]

57. Savio, R.L.; Miritello, M.; Cardile, P.; Priolo, F. Concentration dependence of the Er^{3+} visible and infrared luminescence in $Y_{2-x}Er_xO_3$ thin films on Si. *J. Appl. Phys.* **2009**, *106*, 043510. [CrossRef]

58. Savio, R.L.; Miritello, M.; Iacona, F.; Piro, A.M.; Grimaldi, M.G.; Priolo, F. Thermal evolution of Er silicate thin films grown by rf magnetron sputtering. *J. Phys. Condens. Matter* **2008**, *20*, 454218. [CrossRef]

59. Wang, B.; Zhou, P.Q.; Wang, X.J.; He, Y.D. A low-fabrication-temperature, high-gain chip-scale waveguide amplifier. *Sci. China Inform. Sci.* **2022**, *65*, 162405. [CrossRef]

60. Guo, R.; Wang, X.; Zang, K.; Wang, B.; Wang, L.; Gao, L.; Zhou, Z. Optical amplification in Er/Yb silicate strip loaded waveguide. *Appl. Phys. Lett.* **2011**, *99*, 161115. [CrossRef]

61. Wang, L.; Guo, R.; Wang, B.; Wang, X.; Zhou, Z. Hybrid Si_3N_4-Er/Yb Silicate Waveguides for Amplifier Application. *IEEE Photonic Tech. L.* **2011**, *24*, 900–902. [CrossRef]

62. Guo, R.; Wang, B.; Wang, X.; Wang, L.; Jiang, L.; Zhou, Z. Optical amplification in Er/Yb silicate slot waveguide. *Opt. Lett.* **2012**, *37*, 1427–1429. [CrossRef]

63. Zhou, P.; Wang, X.; He, Y. A sub-kHz narrow-linewidth, and hundred-mW high-output-power silicon-based Er silicate laser with hybrid pump and signal co-resonant cavity. *IEEE Photonics J.* **2020**, *12*, 1500212. [CrossRef]

64. Zhou, P.; Wang, X.; He, Y.; Zou, W. A high-power, high-efficiency hybrid silicon-based Er silicate-silicon nitride waveguide laser. *IEEE J. Quantum Elect.* **2020**, *56*, 110111. [CrossRef]

65. Zhou, P.; Wang, B.; Wang, X.; Wang, B.; He, Y.; Bowers, J.E. Design of an on-chip electrically driven, position-adapted, fully integrated Er-based waveguide amplifier for silicon photonics. *OSA Continuum* **2021**, *4*, 790–814. [CrossRef]

66. Boes, A.; Corcoran, B.; Chang, L.; Bowers, J.E.; Mitchell, A. Status and potential of lithium niobate on insulator (LNOI) for photonic integrated circuits. *Laser Photonics Rev.* **2018**, *12*, 1700256. [CrossRef]

67. Qi, Y.F.; Li, Y. Integrated lithium niobate photonics. *Nanophotonics* **2020**, *9*, 1287–1320. [CrossRef]

68. Wang, C.; Zhang, M.; Chen, X.; Bertrand, M.; Shams-Ansari, A.; Chandrasekhar, S.; Winzer, P.; Loncar, M. Integrated lithium niobate electro-optic modulators operating at CMOS-compatible voltages. *Nature* **2018**, *562*, 101–104. [CrossRef] [PubMed]

69. He, M.; Xu, M.; Ren, Y.; Jian, J.; Ruan, Z.; Xu, Y.; Gao, S.; Sun, S.; Wen, X.; Zhou, L.; et al. High-performance hybrid silicon and lithium niobate Mach–Zehnder modulators for 100 Gbit s^{-1} and beyond. *Nat. Photonics* **2019**, *13*, 359–364. [CrossRef]

70. Lu, J.; Surya, J.B.; Liu, X.; Bruch, A.W.; Gong, Z.; Xu, Y.; Tang, H.X. Periodically poled thin-film lithium niobate microring resonators with a second-harmonic generation efficiency of 250,000%/W. *Optica* **2019**, *6*, 1455–1460. [CrossRef]

71. He, Y.; Yang, Q.F.; Ling, J.; Luo, R.; Liang, H.; Li, M.; Shen, B.; Wang, H.; Vahala, K.; Lin, Q. Self-starting bi-chromatic LiNbO3 soliton microcomb. *Optica* **2019**, *6*, 1138–1144. [CrossRef]

72. Jin, H.; Liu, F.M.; Xu, P.; Xia, J.L.; Zhong, M.L.; Yuan, Y.; Zhou, J.W.; Gong, Y.X.; Wang, W.; Zhu, S.N. On-Chip Generation and Manipulation of Entangled Photons Based on Reconfigurable Lithium-Niobate Waveguide Circuits. *Phys. Rev. Lett.* **2014**, *113*, 103601. [CrossRef]

73. Luo, R.; Jiang, H.; Rogers, S.; Liang, H.; He, Y.; Lin, Q. On-chip second-harmonic generation and broadband parametric down-conversion in a lithium niobate microresonator. *Opt. Express* **2017**, *25*, 24531–24539. [CrossRef] [PubMed]

74. Liang, Y.; Zhou, J.; Liu, Z.; Zhang, H.; Fang, Z.; Zhou, Y.; Yin, D.; Lin, J.; Yu, J.; Wu, R.; et al. A high-gain cladded waveguide amplifier on erbium doped thin-film lithium niobate fabricated using photolithography assisted chemo-mechanical etching. *Nanophotonics* **2022**, *11*, 1033–1040. [CrossRef]

75. Li, T.; Wu, K.; Cai, M.; Xiao, Z.; Zhang, H.; Li, C.; Xiang, J.; Huang, Y.; Chen, J. A single-frequency single-resonator laser on Er-doped lithium niobate on insulator. *APL Photonics* **2021**, *6*, 101301. [CrossRef]

76. Cai, M.; Wu, K.; Xiang, J.; Xiao, Z.; Li, T.; Li, C.; Chen, J. Er-doped lithium niobate thin film waveguide amplifier with 16 dB internal net gain. *IEEE J. Sel. Top. Quant.* **2022**, *28*, 8200608. [CrossRef]

77. Moss, D.J.; Morandotti, R.; Gaeta, A.L.; Lipson, M. New CMOS-compatible platforms based on silicon nitride and Hydex for nonlinear optics. *Nat. Photonics* **2013**, *7*, 597–607. [CrossRef]

78. Liu, J.; Huang, G.; Wang, R.N.; He, J.; Raja, A.S.; Liu, T.; Engelsen, N.J.; Kippenberg, T.J. High-yield, wafer-scale fabrication of ultralow-loss, dispersion-engineered silicon nitride photonic circuits. *Nat. Commun.* **2021**, *12*, 2236. [CrossRef]

79. Romero-Garcia, S.; Merget, F.; Zhong, F.; Finkelstein, H.; Witzens, J. Silicon nitride CMOS-compatible platform for integrated photonics applications at visible wavelengths. *Opt. Express* **2013**, *21*, 14036–14046. [CrossRef]

80. Munoz, P.; Mico, G.; Bru, L.A.; Pastor, D.; Perez, D.; Domenech, J.D.; Fernandez, J.; Banos, R.; Gargallo, B.; Alemany, R.; et al. Silicon nitride photonic integration platforms for visible, near-infrared and mid-infrared applications. *Sensors* **2017**, *17*, 2088. [CrossRef]